Copper ESEEM and HYSCORE through ultra-wideband chirp EPR spectroscopy

Journal Article

Author(s):
Segawa, Takuya Fabian (iD); Doll, Andrin; Pribitzer, Stephan; Jeschke, Gunnar

Copper ESEEM and HYSCORE through ultra-wideband chirp EPR spectroscopy

Takuya F. Segawa,[1] Andrin Doll,[1] Stephan Pribitzer,[1] and Gunnar Jeschke[1, a]

ETH Zurich, Laboratory of Physical Chemistry, Vladimir-Prelog-Weg 2,

CH-8093 Zurich, Switzerland

(Dated: 2 June 2015)

———
[a]Electronic mail: gjeschke@ethz.ch.

I.   MONOCHROMATIC PULSE 2D EPR/TWO-PULSE ESEEM SPECTRUM OF THE MALONIC ACID RADICAL
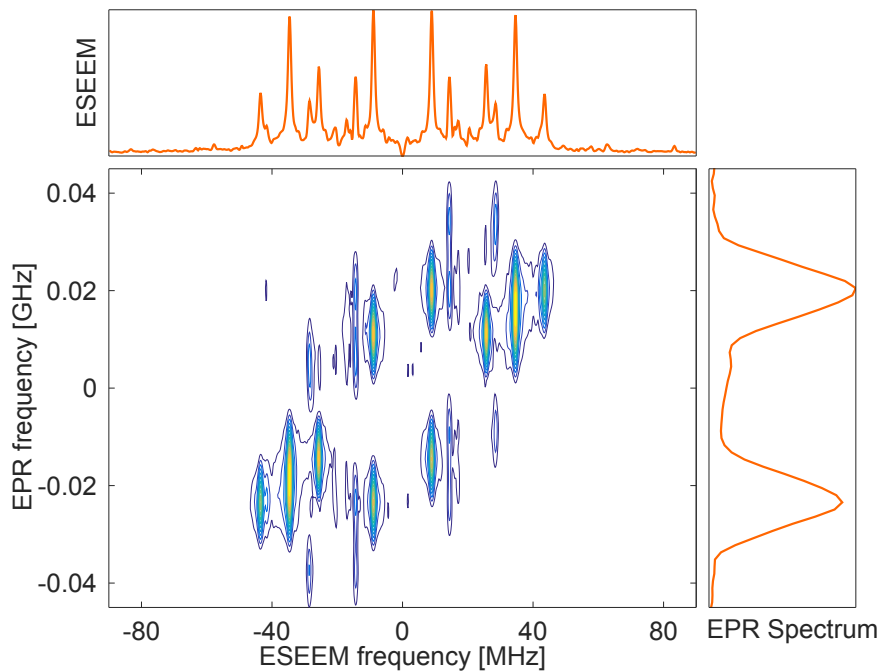

FIG. S1: 2D EPR/two-pulse ESEEM spectrum of a γ-irradiated malonic acid crystal, recorded with a two-pulse sequence of 3.25 ns and 6.5 ns monochromatic rectangular pulses. The spectrum was recorded at the same crystal orientation and the same increment of the delay τ as the chirp 2D EPR/two-pulse ESEEM spectrum in Fig. 1 of the main text. Both sequences generate the same 2D correlation spectrum.

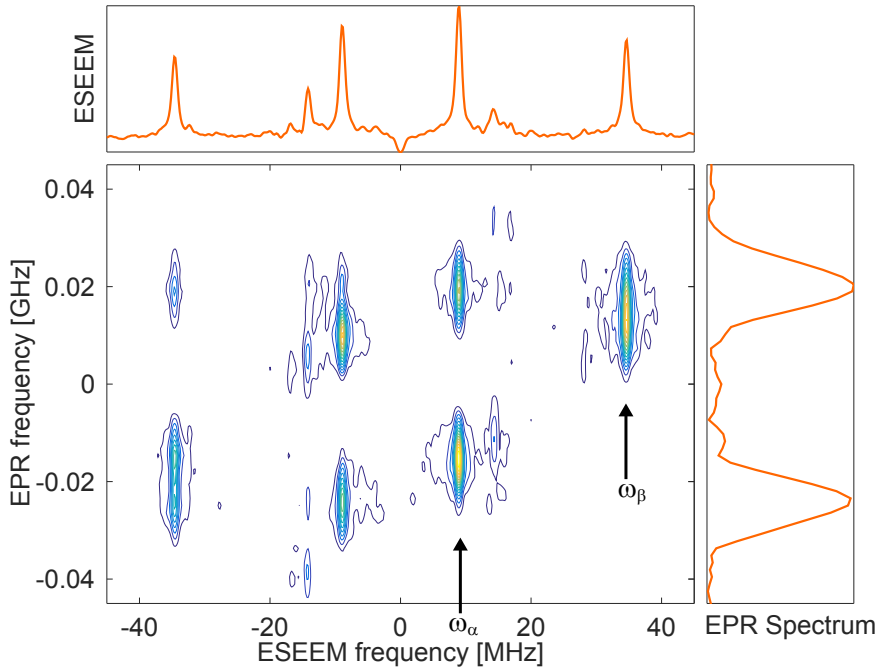## II. CHIRP 2D EPR/THREE-PULSE ESEEM SPECTRUM OF THE MALONIC ACID RADICAL

FIG. S2: 2D EPR/three-pulse ESEEM spectrum of a γ-irradiated malonic acid crystal, recorded with a sequence of 100 ns, 50 ns and 50 ns chirp pulses over a sweep range $\Delta f = +200$ MHz. The spectrum was recorded at the same crystal orientation as the chirp 2D EPR/two-pulse ESEEM spectrum in Fig. 1 of the main text. The first delay τ was set to 960 ns and the delay T was incremented from 1.3 μs to 4.3 μs in steps of 6 ns. In the three-pulse ESEEM spectrum shown here, combination peaks at ω_+ and ω_- disappeared and the linewidths along the ESEEM dimension became narrower. Only the two nuclear transitions $\omega_\alpha/2\pi = 9.0$ MHz and $\omega_\beta/2\pi = 34.7$ MHz and the weaker signals at $\omega_I/2\pi = 14.3$ MHz from more remote matrix protons are visible in this three-pulse ESEEM spectrum. The diagonal shape of the spin echo correlation spectrum is slightly disturbed by the cross peak at the top left of the 2D plot. This asymmetry of the chirp three-pulse correlation spectrum is discussed in the main text looking at the crystal of Cu^{2+} in rutile in Fig. 3. This asymmetric cross peak was not observed for the three-pulse 2D spectrum using monochromatic pulses (not shown), confirming experimentally that it is caused by a passage pulse effect.

III. SIMULATED CHIRP 2D EPR/TWO-PULSE ESEEM SPECTRUM OF Cu^{2+} IN A RUTILE CRYSTAL ALIGNED TO THE MAGNETIC FIELD EXACTLY ALONG THE (110) CRYSTAL AXIS
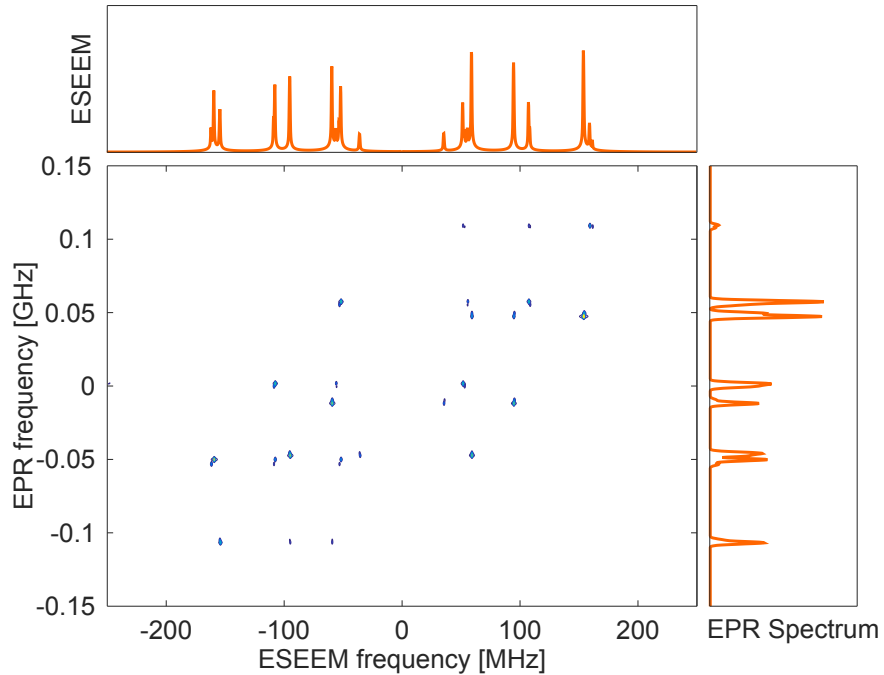

FIG. S3: Simulated 2D EPR/two-pulse ESEEM spectrum of a Cu^{2+} in a rutile crystal with a sequence of 128 ns and 64 ns pulse duration over a sweep range of 500 MHz. A magnetic field exactly perpendicular to the (110) surface was assumed. The simulation is based on the Hamiltonian parameters in Brant et al. (Ref. [22] in the main text), as in Fig. 2b of the main text. In the orientation along a principal axis of the Hamiltonian considered here, only forbidden transitions with $\Delta m_I = \pm 2$ and no lines from $\Delta m_I = \pm 1$ appear. Therefore, additional EPR peaks in Fig. 2 of the main text must stem from $\Delta m_I = \pm 1$ and $\Delta m_I = \pm 3$ transitions, introduced by a slight rotation away from the principal axis. Accordingly, an increased number of ESEEM transitions is observed.

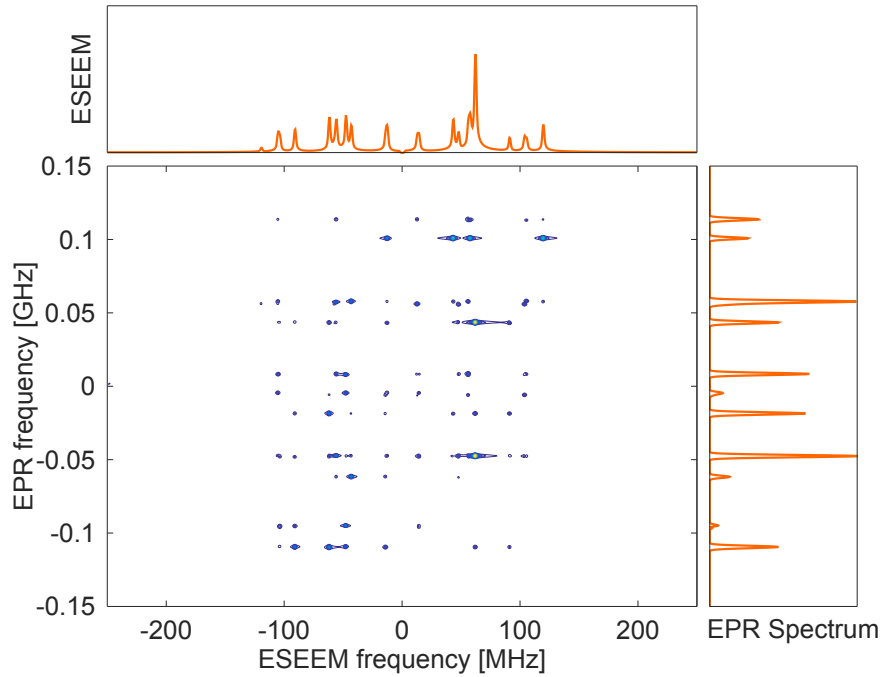## IV.   SIMULATED MONOCHROMATIC PULSE 2D EPR/THREE-PULSE ESEEM SPECTRUM OF Cu^{2+} IN A RUTILE CRYSTAL

FIG. S4: Simulated 2D EPR/three-pulse ESEEM spectrum of a Cu^{2+} in a rutile crystal assuming ideally non-selective pulses that cover the full spectral range. The orientation for the simulation is the same as in Fig. 2 and 3 in the main text. In contrast to the experimental and simulated chirp three-pulse ESEEM spectra in Fig. 3 of the main text, this 2D spectrum does not show the pronounced asymmetry with respect to the diagonal.

No perfect symmetry is observed, since the EPR spectrum itself is not symmetric.

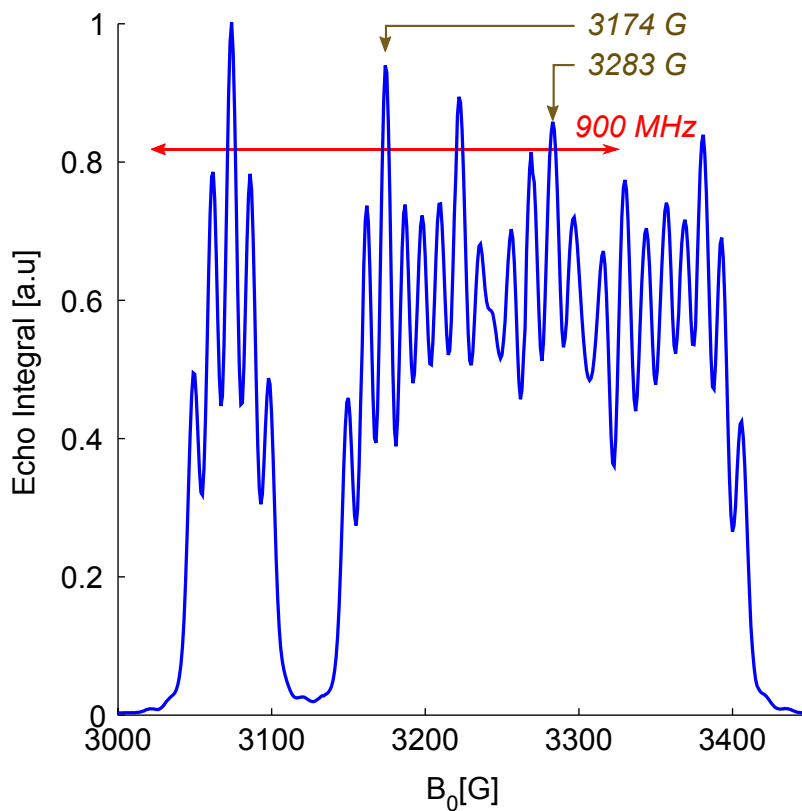## V. ECHO-DETECTED FIELD SWEEP EPR SPECTRUM OF A BISPICOLINATE CU(II) CRYSTAL

FIG. S5: Echo-detected field sweep of the bispicolinate Cu(II) Cu(pic)$_2$ crystal in the same orientation as for all experiments on this sample in the main text (see Fig. 5 and 6) at a microwave (mw) frequency of 9.5 GHz. The peaks appearing at the two magnetic fields B_0 of 3174 G and 3283 G that were used for the ultra-wideband chirp experiments are indicated in the spectrum.

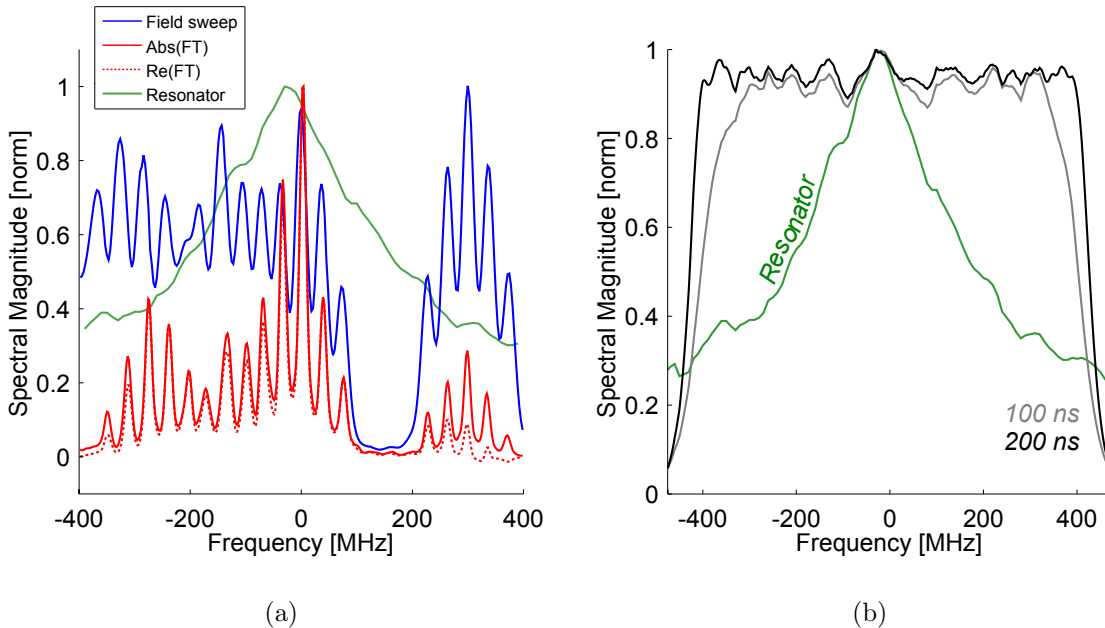# VI. RESONATOR-INDUCED BANDWIDTH LIMITATIONS FOR THE BISPICOLINATE CU(II) CRYSTAL

(a)   (b)

FIG. S6: Influence of the resonator bandwidth on the UWB chirp experiments. (a) Comparison between a field-swept echo-detected EPR spectrum of Cu(pic)$_2$ (blue) and a FT-chirp echo EPR spectrum at 3174 G (converted to a frequency scale) using a 200 ns $\pi/2$-pulse and 100 ns π-pulse swept over 950 MHz (red). Comparison of the absolute value spectrum (solid red line) with the absorption spectrum (dotted red line) reveals slight offset-dependent phase deviations. The normalized mw field B_1 at the sample postion as a function of the offset is plotted in green. (b) Compensation of the non-uniform resonator profile by offset-independent adiabaticity pulses. Besides the normalized resonator profile (green), the FT excitation profiles (see Ref. [9] and [11] in the main text) of the 200 ns pulse (black) and the one of the 100 ns pulse (grey) are shown. This compensation scheme works better for pulses with longer duration, as it is illustrated by the slightly smaller uniform excitation bandwidth of the 100 ns pulse.

VII. CHIRP ULTRA-WIDEBAND 2D EPR/THREE-PULSE ESEEM SPECTRUM OF A BISPICOLINATE CU(II) CRYSTAL
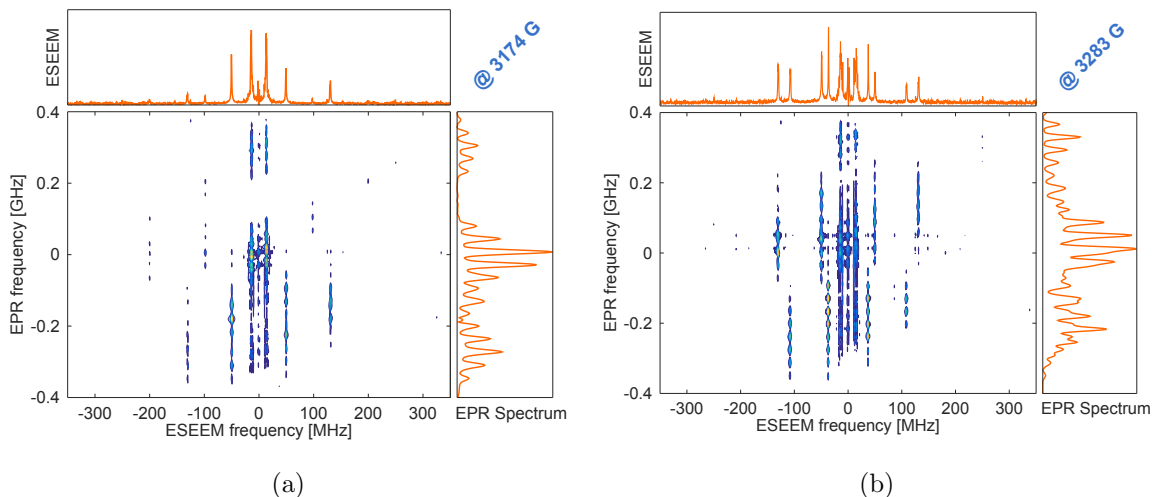

(a)   (b)

FIG. S7: Experimental 2D EPR/three-pulse ESEEM spectra of a ^{63}Cu(pic)$_2$ crystal. A sequence with pulse lengths of 200 ns, 100 ns and 100 ns and a frequency sweep range of $\Delta f = +900$ MHz was used. The first delay τ was set to 250 ns and the delay T was incremented from 0.35 μs to 4.35 μs in steps of 1 ns. To cover the complete EPR spectrum, (a) was recorded at a magnetic field of $B_0 = 3174$ G and (b) at 3283 G. By comparison with the corresponding 2D spectra in Fig. 5 of the main text, remaining basic nuclear frequencies and missing combination frequencies can be identified. The basic nuclear frequencies in these spectra are then correlated in the HYSCORE spectra of Fig. 6 in the main text.